The dynamics and structure of forecast error covariance in the inner core of a developing hurricane.

Jonathan Poterjoy and Fuqing Zhang

1. Introduction

Improvements have been made over the past three decades in our ability to forecast the track of tropical cyclones (TCs) (Franklin et al. 2009), which is primarily determined by synoptic-scale environmental flow (Wu and Emanuel 1993; Wu and Kurihara 1996; Wang et al 1998). Despite this progress, our ability to accurately predict intensity change remains quite limited (Elsberry et al. 2007; Houze et al. 2007). The inner-core region of a TC is governed by a multi-scale array of dynamic and thermodynamic processes in an air-sea coupled environment. Operational intensity prediction can be substantially improved by adopting high-resolution convective scale models, and advanced vortex initialization through a more refined use of dropsondes and remotely sensed observations (Leidner et al. 2003; Burpee et al. 1996). Despite such optimism, it is apparent that our inability to initialize a TC with dynamically consistent structure and intensity remains a limiting factor for short to medium-range operational storm prediction. More specifically, small-scale errors associated with moist convection often propagate into large-scale model errors in time (Hendricks et al. 2004; Krishnamurti et al. 2005; Montgomery et al. 2006; Zhang and Sippel 2009). This issue stresses the importance of optimal state estimation, also known as data assimilation; where observations, a previous model forecast (background) and their respectable errors are used to estimate a model state prior to integration that contains the least amount of error.

Data assimilation is performed via a *variational* method in which a cost function measuring the distance between a prior forecast and observations is minimized to find the *analysis* state, or by a secondary approach in which an *innovation* or correction is added to the background state vector after assigned an optimal weight in a *least squares* approach (Talagrand 1997). The process of state estimation requires knowledge of both observational and forecast error statistics in terms of variance and covariance. Covariance not only provides an estimate of forecast uncertainty, but also quantifies linear relationships within the model state, allowing information to be shared between like and unlike variables. In essence, forecast error covariance determines the extent to which a measured variable can correct state variables in model space. Rather than using stationary, isotropic background error covariance, as is the case for variational data assimilation systems, a least squares approach called the Ensemble Kalman filter (EnKF) takes into account flow-dependent covariance, estimated from an ensemble of short-range forecasts.

Model initialization using an EnKF has gained much ground in regional and mesoscale prediction in recent years (e.g. Snyder and Zhang 2003; Zhang et al. 2004; Dowell et al. 2004; Tong and Xue 2005; Zhang et al. 2006; Torn et al. 2006; Meng and Zhang 2007; Fujita et al. 2007; Meng and Zhang 2008a,b), and has proven successful on several TC case studies without the use of vortex bogussing (Chen and Snyder 2007; Torn and Hakim 2009; Zhang et al. 2009). In particular, recent case studies in which the EnKF was used to assimilate Doppler radar radial velocity observations into the Weather Research and Forecasting model (WRF) demonstrated promising results (Zhang et al. 2009).

Bearing in mind the importance of non-static, flow-dependent forecast error for dynamically consistent TC initialization; this research is dedicated entirely to the study of state variable covariance in the inner-core region of a mature hurricane. Coherent correlation structures that arise from TC forecast error growth were examined using an ensemble of forecasts from the Weather Research and Forecasting model (WRF) for Hurricane Katrina as it intensified from a tropical storm to a category 4 hurricane. For comparison, correlations were also calculated from the axisymmetric hurricane model developed in Rotunno and Emanuel 1987. An ensemble intensity comparison for the two models is provided in figures 1a-b.

We explored several features of ensemble forecasts that lead to anisotropic covariance within the inner-core region of a tropical cyclone; i.e. vortex asymmetry, tilting, size, intensity, and position error. In

Jonathan Poterjoy
Pennsylvania State University, State College, PA, email: jpoterjoy@psu.edu

Fuqing Zhang
Pennsylvania State University, State College, PA, email: fzhang@psu.edu

the following section, a brief description of our WRF configuration and ensemble generation are provided. The motivation behind our choice of statics is discussed in section three. Section four provides several examples demonstrating how the flow-dependent model dynamics evolve forecast variance and correlations in time, and the last section serves as a summary and conclusion.

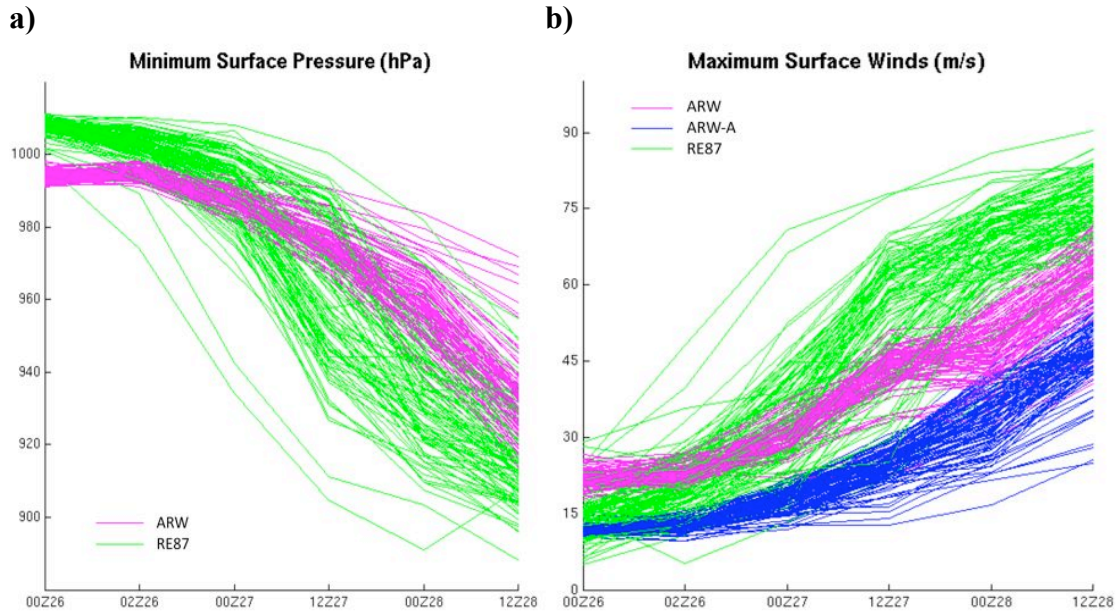

Fig. 1 *Minimum sea level pressure (a) and Maximum wind speeds (b) are shown for ARW and RE87 model ensembles. ARW-A (blue lines) represent the maximum surface wind speed after azimuthal averaging. Values are plotted at 12-h intervals for ARW output, and 24-h intervals for RE87. Since RE87 requires a longer spin-up time, each 24-hr RE87 forecast increment is plotted next to a 12-h ARW increment for better comparrison.*

2. Forecast model and experiment descriptions

2.1 Advanced Research WRF

The Advanced Research WRF (ARW) is a fully compressible, nonhydrostatic, convective scale model that uses an Arakawa-C grid and vertical levels that follow terrain using hydrostatic pressure (Skamarock et al. 2005). WRF version 3.11 was used for this experiment with a course domain of 202×181 horizontal grid points at 40.5 km grid spacing, and two two-way nested domains that automatically follow the storm using the WRF vortex following algorithm. The innermost domain (D3), where all analysis for this experiment is performed, has 34 vertical levels and follows the vortex using a 253 x 253 horizontal grid with a spacing of 4.5 km. See Zhang et al. 2009 for the selection of physical parameterization schemes.

An ensemble of 100 forecasts of Hurricane Katrina with a lead-time of 64 hours was produced following several hours of EnKF assimilation of airborne radar data. Forecasts were initialized from EnKF analysis members at 2000 UTC 25 August 2005 and ensemble error statistics were calculated every 6 hours, beginning 0000 UTC 26 and ending 1200 UTC 28. The dynamic and thermodynamic structure of Katrina members changed dramatically during the simulated time period, as a majority progressed from tropical storm intensity at the time of initialization to category 4 hurricanes by the end of the forecast.

In this study, Lagrangian correlation structures, i.e. relationships between measurable variables and state variables relative to a frame of reference following a vortex, and Eulerian correlations, calculated with respect to a static location, are used for analyzing the ensemble error propagation throughout the forecast. Post-processing of D3 model output was performed in the following manor:

1. Each member was repositioned based on the location of minimum sea level pressure such that the centers of each vortex are aligned at the lowermost model level. This step removes storm

track errors and allows for simple Lagrangian reference frame calculations. Experiments in which correlations are estimated immediately after this post-processing step are named ***ARW-L***.

2. Following the previous step, model output from each member was averaged azimuthally to remove high wavenumber asymmetries in Katrina member vortices for a second experiment called ***ARW-LA***.
3. To perform an Eulerian reference frame analysis, members were relocated based on the 6-hr ensemble track spread in a method that preserved the forecasted mean vortex position (Fig. 2a-b). In doing so, the ensemble contains the same position error at all time steps, consistent with a hypothetical 6-hr analysis cycle. This method was also used to introduce position errors in the steady-state vortex model described in the following section. Experiments in which position errors are rescaled via this method for the ARW ensemble are named ***ARW-E***.
4. In the last post processing step, model output was azimuthally averaged about the location of minimum sea level pressure (see step 2) and relocated based on 6-hr ensemble track spread (see step 3). This results in a wavenumber zero, Eulerian reference frame case called ***ARW-EA***.

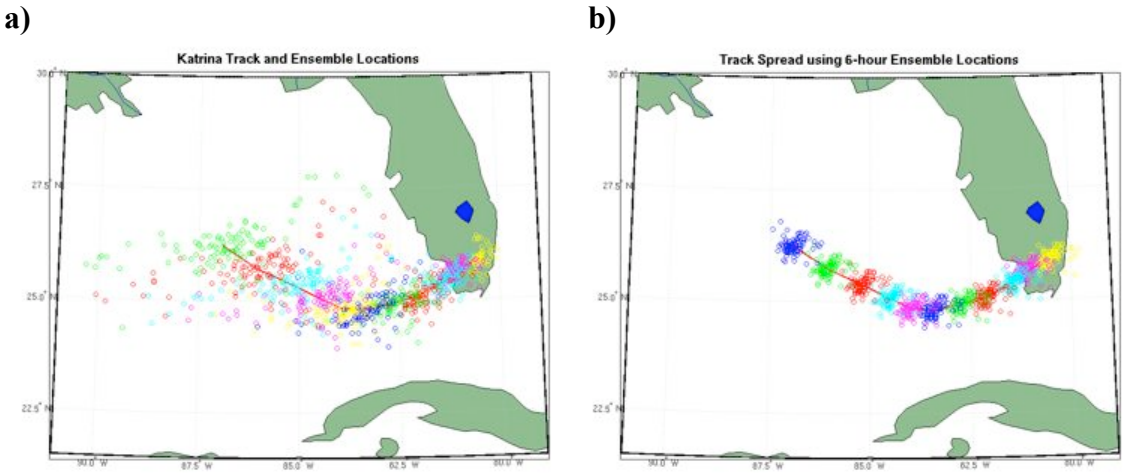

Fig. 2 *Ensemble vortex positions (a) and rescaled positions (b) are plotted along with the mean forecasted track. The rescaled track spread is calculated from 6-h ensemble vortex positions.*

Since the region of interest in our case lies within the vicinity of the hurricane's eye, all calculations are performed in a subspace of D3, which will be referred to as S. The new subspace, S, has a grid size of 89 x 89 x 30 and roughly covers a 400 x 400 x 18 km^3 area, and restricts our investigation to the inner-core region of the hurricane, where dynamic and thermodynamic relationships are often poorly represented by parameterized covariance.

2.1 Rotunno-Emanuel (1987) axisymmetric hurricane model

The model described in this section (herein denoted as RE87) was used in Rotunno and Emanuel (1987) for studying the maximum potential intensity of a tropical cyclone, given a neutral atmospheric sounding of temperature and humidity, and a sea surface temperature. It is an adaptation of a model originally designed by Klemp and Wilhelmson (1978) to study cumulus clouds, and further developed by Willoughby et al. (1984) for tropic cyclone research. The RE87 equations are for compressible, nonhydrostatic, axisymmetric flow on an *f*-plane, using cylindrical coordinates. The model is initialized using a finite amplitude vortex, specified by a maximum tangential wind speed (V_o), radius of maximum winds (R), and radius of zero wind, which develops into a steady-state vortex over time. To allow for a horizontal and vertical depiction of the vortex, the authors interpolated RE87 output from two-dimensional (*r-z* plane) spherical coordinates to a three-dimensional Cartesian domain. Random perturbations were added to V_o and R to generate a 100-member ensemble of vortices, which will be used to estimate a correlation matrix. An atmospheric sounding and mean sea surface temperature for each member were calculated from individual ARW members at 12 UTC 28 August, thus allowing each vortex to develop in

the same environment as Katrina. Through previous experiments, the authors observed that little change typically occurs in correlation structures for RE87 when a higher model resolution is used, a result that is consistent with the findings of Gao and Xue 2008 and Yang and Kalnay 2008 using higher-order atmospheric models. This justified the use of a courser, 9 km grid spacing for RE87 to speed the generation of ensemble vortex simulations.

3. Ensemble correlations and variance

The flow-dependent nature of forecast covariance is a byproduct of the underlying error growth dynamics, as alluded by Cohn and Parish (1991), Daley (1992), Evensen (1994), and Zhang (2005). Besides the practical use of covariance for operational data assimilation, model forecast error calculated from ensembles provides a wealth of dynamical information about the geophysical system at hand. When covariance is used for this purpose, it is beneficial to dissect the statistic into the components of correlation and variance. Correlations indicate how information is shared between like and unlike variables in both space and time, while variance isolates the location of largest model uncertainty for a given event.

Correlation is the normalized value for covariance, and is given by:

$$Corr(x_{ijk}, y_{lmn}) = \frac{Exp[(x_{ijk} - \bar{x}_{ijk})(y_{lmn} - \bar{y}_{lmn})]}{\sigma_x \sigma_y} = \frac{Cov(x_{ijk}, y_{lmn})}{\sigma_x \sigma_y}$$

where x and y represent two state variables at model grid points (i,j,k), and (l,m,n) respectively. Terms denoted with an overbar are ensemble means and σ represents sample standard deviations for variables x and y. A cross-spatial correlation will refer to a correlation between two unlike variables, calculated with respect to a constant correlation point $[x \neq y,\ (i,j,k) \neq (l,m,n)]$, as shown by the *2 x 2* matrix

$$\begin{bmatrix} r(x_{22}, y_{11}) & r(x_{22}, y_{12}) & r(x_{22}, y_{13}) \\ r(x_{22}, y_{21}) & r(x_{22}, y_{22}) & r(x_{22}, y_{23}) \\ r(x_{22}, y_{31}) & r(x_{22}, y_{32}) & r(x_{22}, y_{33}) \end{bmatrix},$$

where element (*2,2*) is chosen as the location of interest. In terms of data assimilation, the cross-spatial correlation matrix is used to spatially propagate information from an observed scalar quantity to model state variables. Estimates of uncertainty for the measured and modeled variables are provided by known observation error and the estimated forecast variance respectively, which is used to determine the optimal weight associated with each independent estimate of the model state. Forecasters and dynamicists can also use ensemble error pragmatically for quantifying the degree of predictability associated with a given event.

4. Results

The principal dynamical features of TCs are the secondary circulation, characterized by a shallow layer of radial inflow near the surface and cold outflow in the upper troposphere, convergence and moist adiabatic accent in the eyewall, and weak subsidence in the eye (Liu et al. 1999). Intense temperature gradients, moist convection, and the warm temperature anomaly at mid levels are also defining attributes of the inner-core region (Shea and Gray 1973). Forecast uncertainty and correlations are primarily determined by the circulation's response to ensemble spread in storm intensity, size, location, and degree of organization (i.e symmetry and tilt) of individual Katrina members.

After each analysis using the EnKF, an ensemble of initial model states is made available for generating the forecast ensemble. Our last analysis cycle occurs on 20 UTC 25 August, a time at which Katrina strengthened to tropical storm intensity. The 20 UTC analysis ensemble contains only marginal amounts of spread, and significant large-scale correlations between minimum sea level pressure (*minSLP*) and meridional wind (v) (fig. 3ab). The initial ensemble shows a weak, but dynamically consistent mean vortex as the pressure gradient force is largely in balance with the wind field. Variance in the v analysis, although small, is focused primarily in the center of domain S and is most likely a result of vortex position errors imposed on the ensemble.

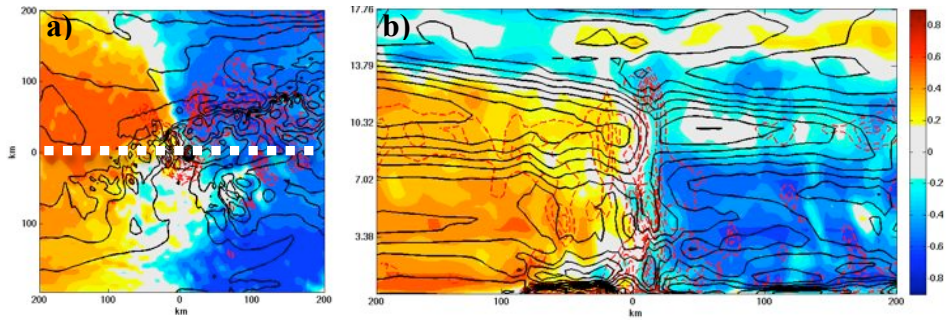

Fig. 3 *Analysis cross-spatial correlations of minSLP and v are plotted with contours of maximum variance (red) ranging from 4.6 – 18.4 m^2s^{-2}, and mean v (black). Figure A is a horizontal plot for the surface level, while figure b is a vertical cross section through the dashed line indicated on figure a.*

After four hours of model integration, the 00 UTC 26 forecast ensemble statistics are shown in figures 4ab. For a hypothetical situation in which the EnKF analysis/forecast cycles were allowed to carry through to future time steps, covariance calculated from the resulting values would be used to correct the *v* field using a measurement of *minSLP*. During integration, the initial variance maximum originally located at the mean vortex center is now displaced to the eastern wall of S, near a local maximum in *v* (fig. 4ab). Changes also occur in the magnitude and location of *minSLP*-*v* correlations, as they diminish slightly between the two time steps. A smaller balance between pressure gradient and wind velocity is present everywhere in S at 00 UTC 26, showing a shift from the largely balanced initial vortices to more complicated structures that deviate from the largely symmetric initial wind field. Hydrostatic and geostrophic adjustments occurring immediately after the analysis may also result from imbalances present in the initialized model state, and present a significant influence on initial forecast error growth. It is apparent that errors in wind velocity outweigh position errors at this forecast time, resulting in a new variance maximum outside the vortex core region.

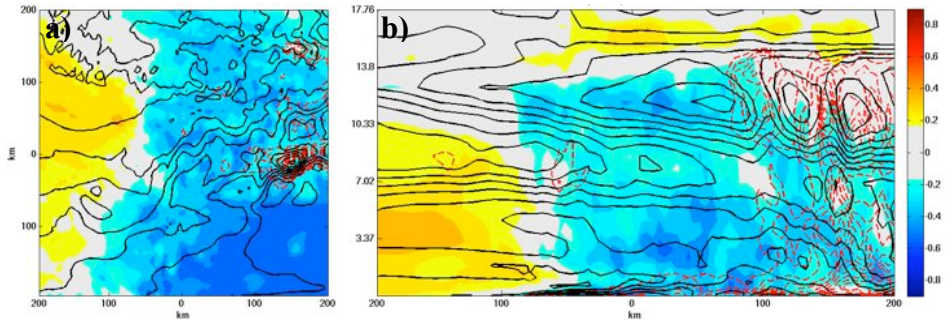

Fig. 4 *4-h forecast cross-spatial correlations of minSLP and v are plotted with contours of maximum variance (red) ranging from 10.0 – 39.9 m^2s^{-2}, and mean v (black). Both cross sections are through the same region described in Fig. 3.*

Consistent with findings from Zhang 2005 where ensembles were used to analyze the error growth of a mid-latitude winter cyclone, coherent error structures begin to develop after longer ensemble lead-times. For the remainder of this paper, initial condition imbalances will no longer be a large factor in the succeeding error statistics, as ensemble forecasts of 12-h or more will be the topic of discussion. Given the large ensemble track spread associated with large lead-times, the position rescaling method discussed earlier will be used to mimic an Eulerian reference frame ensemble (ARW-E) for each time step. To separate the effects of storm position and vortex structure errors on the variance and correlation matrices, we will also show calculations performed for Lagrangian reference frame ensembles (ARW-L). Using both the Eulerian and Lagrangian reference frame, members were also averaged azimuthally to determine the wavenumber zero effects of vortex ensemble error (ARW-EA and ARW-LA).

As a tropical cyclone transitions into a mature hurricane, the primary circulation becomes stronger and more organized, leaving the simulated vortices less sensitive to vertical wind shear and other external forcing mechanisms. Figures 5a-h show how forecast error evolves with the underlying model dynamics

while ARW-L members increase from tropical storm to category 4 intensity. Each time step illustrates major structural changes in the ensemble error, which become more organized and centrally localized with time. During early time steps (Figs 5a-f), *minSLP-v* correlations grow from negligible (< |0.2|), loosely organized structures to significant (< |0.6|), geostrophically consistent structures by the time Katrina reaches category 2 intensity. By 12 UTC 28, many of the members have reached category 4 intensity, resulting in the volume of significant correlations contracting to a region that encompasses only the inner core (Figs 5g-h). Ensemble wind field variance also transitions into tightly organized, symmetric structures with time, as vortex tilt and asymmetry dominates the ensemble error early on in the forecast. Hurricane vortices become more stable and vertically symmetric, allowing errors in ensemble intensity to dominate the contours of maximum variance, since uncertainties in forecasted wind speed dominate structural asymmetries associated with vertical tilt at later time steps.

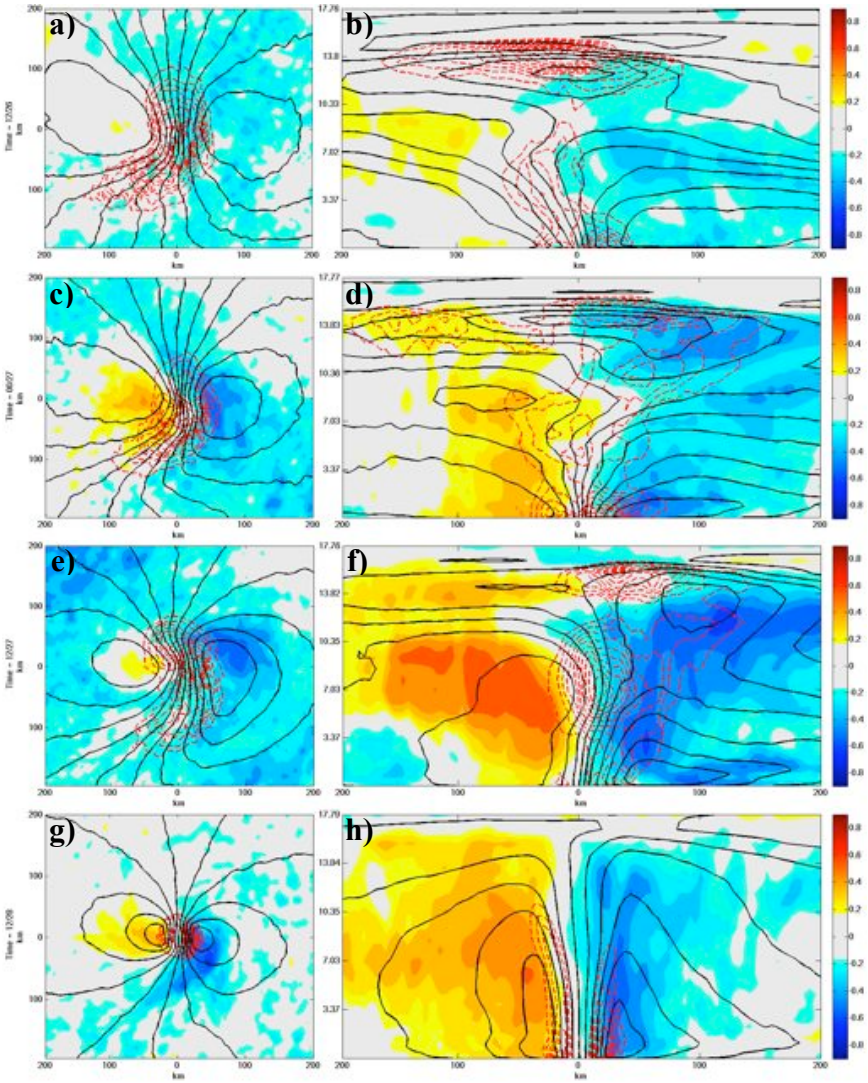

Fig. 5 *ARW-L cross-spatial correlations of minSLP and v are plotted with contours of maximum variance (red), and mean v (black) for 12 UTC 26 (a & b), 00 UTC 27 (c & d), 12 UTC 27 (e & f), and 12 UTC 28 (g & h). Cross sections are through the same region described in Fig. 3.*

When 6-h position errors are imposed on the forecast ensemble at 00 UTC 27 (same time step as Figs 5b-c) in the ARW-E experiment (Figs. 6a-b), little change in *minSLP-v* correlations occur due to *minSLP* being a Galilean invariant quantity. On the other hand, position error causes contours of maximum

variance to be concentrated closer to the origin and surface layers of the ensemble as vortex track spread introduces forecast errors that overwhelm wind field uncertainty introduced by vortex tilting.

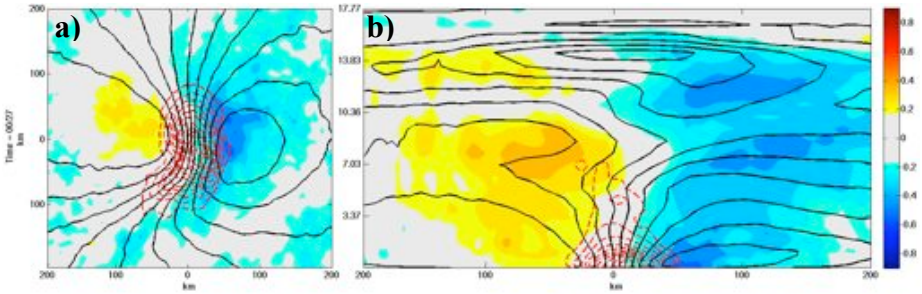

Fig. 6 *Same as Figs. 5c-d, but for ARW-E.*

For cases where the observed variable depends on storm position, correlations are no longer insensitive to position error. Figures 7a-d show a hypothetical situation in which a measured surface tangential wind speed (V_Θ) can be used to correct the temperature field during an EnKF analysis. In this case, V_Θ at a surface point located 27 km from the vortex origin is correlated cross-spatially with perturbation temperature (T) at 12 UTC 28. ARW-L ensemble correlations are largely symmetric at this time step, where a strong, thermally indirect secondary circulation persists. The correlation point is chosen at a location near the radius of maximum winds (*RMW*), thus ensemble intensity spread is the primary cause of the resulting error structures. Members with strong surface wind speeds near the *RMW* coincide with stronger low-level horizontal convergence and moist adiabatic ascent in the eyewall, with forced subsidence and warming in the core; therefore, a column of positive correlations exists inside the hurricane eye, extending from the surface to uppermost levels of S. Error structures that emerge from the ARW-E members at 12 UTC 28 are strikingly different those calculated from ARW-L, as vortex position spread introduces a positive-negative correlation dipole, centered over the measurement location (Figs. 6c-d). These results are consistent with the findings of Chen and Snyder (2007), where non-Gaussian position displacements introduce analysis increment dipoles when forecasted position error is comparable to the vortex size.

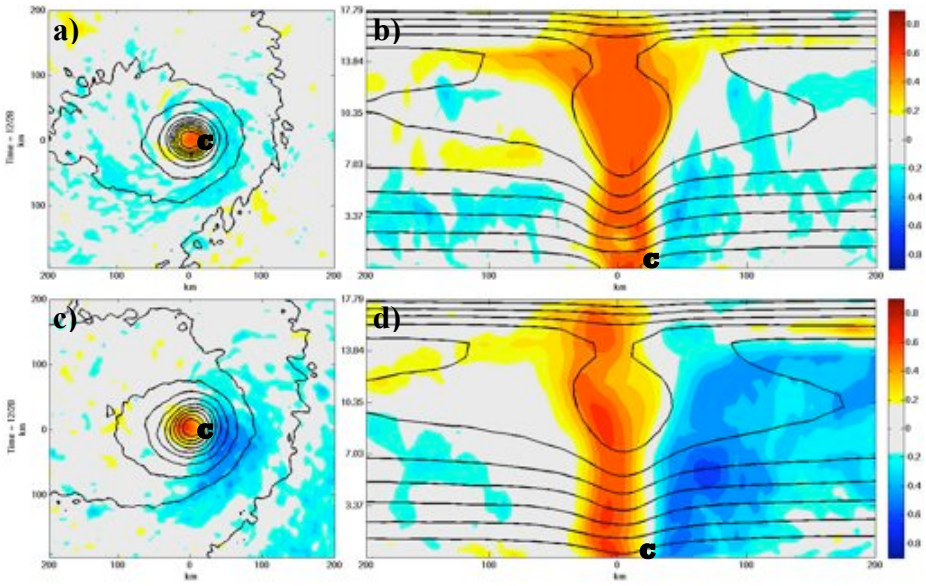

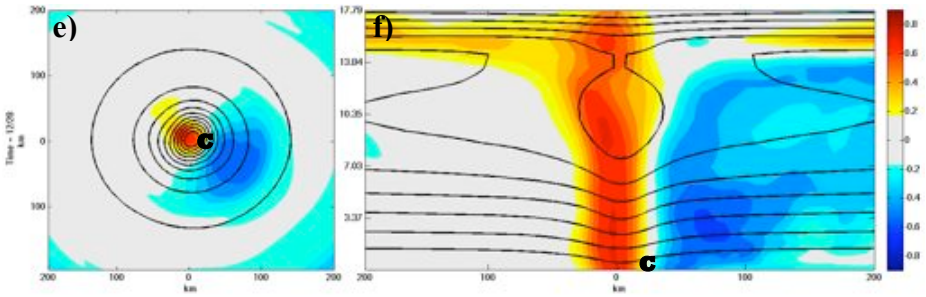

Fig. 7 *Cross-spatial correlations with respect to surface V_θ and the T field for a location marked by '**c**' are plotted with contours of mean T (black) at 12 UTC 28 for ARW-L (a & b), ARW-E (c & d), and ARW-EA (e & f). Cross sections are through the same region described in Fig. 3.*

The resulting dipole correlations have a large dependence on the shape of the ensemble position distribution, since the dipole is oriented diagonally northwest to southeast at the surface, as well as the wavenumber zero structure at large storm intensity, shown in figure 7e-f. This result begs the question of whether or not a simplified, axisymmetric model can reproduce a similar error structure. To investigate the matter, the axisymmetric RE87 model was adopted as a simple and straightforward alternative to the wavenumber zero case shown in figure 7fe-f. Figure 8 shows the evolution of V_Θ - T cross-spatial correlations for a surface point located 36 km from the vortex center. The correlation point was chosen at a larger radius for this example, since weaker vortices at early time steps coincide with greater *RMW*. It is clear that RE87 fails to resolve the same signal at 12 UTC 26, where the ensemble hasn't yet reached hurricane intensity, but as the ARW-E ensemble progresses forward in time, the two models converge toward similar structures. By 00 UTC 28, errors introduced by vortex tilt and small-scale features are negligible in comparison to position error, resulting in ARW-E correlations that are structurally upright and extend to the uppermost layers of domain S. With the exception of magnitude differences, the regional peaks in positive and negative correlations are similar for the two models when vertical sheer is no longer a significant factor governing the flow-dependent error dynamics.

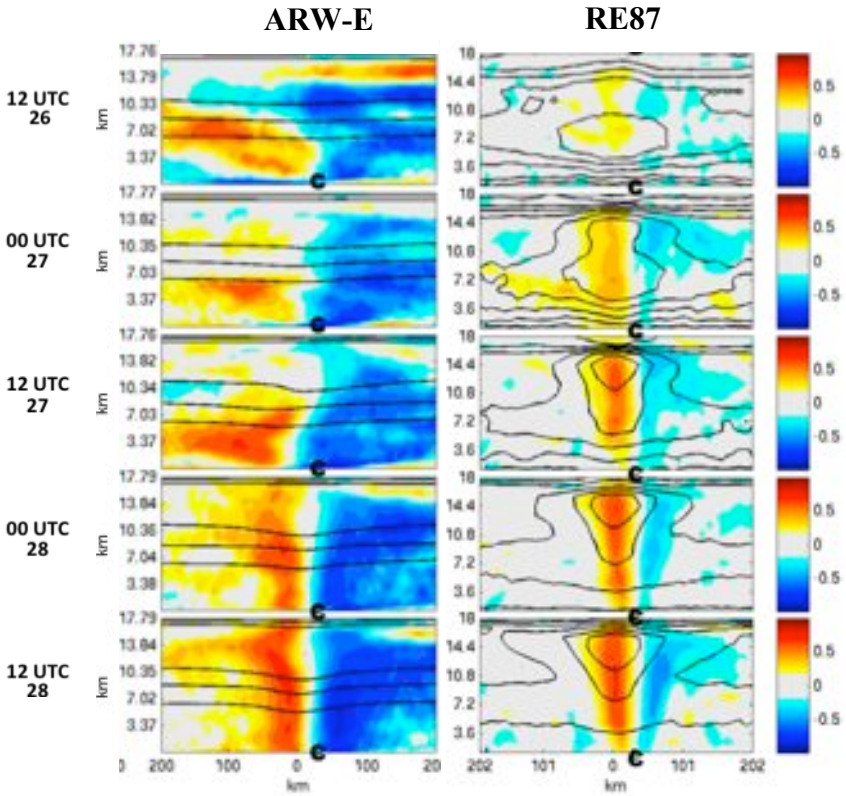

Fig. 8 *Cross-spatial correlations with respect to surface V_θ and the T field for a location marked by '**c**' are plotted with contours of mean T (black) at the time steps indicated on the left for ARW-E and RE87. Cross sections are through the same region described in Fig. 3.*

5. Summary and Conclusion

In an effort to improve our current understanding of ensemble forecast error, correlation and variance structures were analyzed from a 100-member ARW ensemble of Hurricane Katrina during a 64-h period in which forecasts progressed from tropical storm to category 4 hurricane intensity. The observed error statistics were shown to be dependent on initial condition imbalances, storm structure, intensity and position. As simulated vortices increased in intensity, the resulting error was less affected by high wavenumber asymmetries and had a larger dependence on position error.

Since the distribution of vortex positions and wavenumber zero structures were shown to have the largest influence on the ARW ensemble during later time steps, the Rotunno-Emanuel (1987) vortex model was used to estimate the same state variable relationships. Random Gaussian errors with zero mean were added to the initial conditions of RE87 prior to model integration and coherent error structures developed after an ensemble lead-time of five days. Our examination for both model experiments was restricted to a 400 x 400 x 18 km^3 model subspace that captured the inner-core errors and resulting correlations. Previous research (e.g. Houze et al. 2007; Chen et al. 2007; Davis et al. 2008) suggests that the dynamical features of this region may have a profound influence on intensity fluctuation, intensification and decay. Our study was motivated by the small to large-scale error propagation that occurs when inner-core features of an initialized TC vortex are structurally inconsistent, or ill-accounted for during model analysis time steps.

Our results demonstrate how a better understanding of TC error growth dynamics, and linear predictor relationships for complex regions, such as the inner-core, can be achieved through analysis of both high- and low-order forecast ensembles. The structural similarities between ARW and RE87 correlations also suggest that a low-order, two-dimensional model may be developed as a computationally inexpensive alternative to estimating flow-dependent covariance for TC data assimilation under ideal conditions in which an intense tropical cyclone already persists in the background flow field. Since ensemble data assimilation systems have the disadvantage of having to integrate O(100) model states for adequate background error estimation, this approach would eliminate the astringent efforts currently used when high-resolution, cloud resolving models are applied for TC prediction. Such a method would also provide a means of introducing flow-dependent error into a variational data assimilation algorithm.

References:

Burpee, R. W., S. D. Aberson, J. L. Franklin, S. J. Lord, and R. E. Tuleya, 1996: The impact of Omega dropwindsondes on operational hurricane track forecast models. *Bull. Amer. Meteor. Soc.,* **77,** 925-933.

Chen, S. S., J. F. Price, W. Zhao, M. A. Donelan, and E. J. Walsh, 2007: The CBLAST- Hurricane Program and the next-generation fully coupled atmosphere-wave-ocean models for hurricane research and prediction. *Bull. Amer. Meteor. Soc.*, **88**, 311-317

Chen, Y. and C. Snyder, 2007: Assimilating vortex position with an ensemble Kalman filter. *Mon. Wea. Rev.,* **135**, 1828–1845.

Chou, K. H. and C. C. Wu, 2008: Typhoon initialization in a mesoscale model - Combination of the bogused vortex and the dropwindsonde data in DOTSTAR. *Mon. Wea. Rev.,* **136**, 865-879.

Cohn S. E. and D. F. Parish, 1991: The behavior of forecast error covariance for a Kalman filter in 2-Dimensions. *Mon. Wea. Rev.,* **119**, 1757-1785.

Daley R., 1992: Estimating model-error covariances for application to atmospheric data assimilation. *Mon. Wea. Rev.,* **120** 1735-1746.

Davis, C. A., and Coauthors, 2008: Prediction of landfalling hurricanes with the advanced hurricane WRF model. *Mon. Wea. Rev.,* **136**, 1990-2005.

Davis, C. A. and S. Low-Nam, 2001: The NCAR-AVWA Tropical Cyclone Bogussing Scheme. *A Report Prepared for the Air Force Weather Agency.*

Dowell, D. C., F. Zhang, L. J. Wicker, C. Snyder, and N. A. Crook, 2004: Wind and thermodynamic retrievals in the 17 May 1981 Arcadia, Oklahoma supercell: Ensemble Kalman filter experiments. *Mon. Wea. Rev.,* **132**,1982-2005.

Elsberry, R.L., Lambert, T.D.B. & Boothe, M.A., 2007: Accuracy of Atlantic and eastern North Pacific tropical cyclone intensity forecast guidance. *Wea. Forecasting*, **22**, 747-762.

Evensen, G., 1994: Sequential data assimilation with a nonlinear quasi-geostrophic model using Monte Carlo methods to forecast error statistics. *J. Geophys. Res.*, **99**, 10143-10162.

Franklin, J. L., 2009: National Hurricane Center verification report. [Updates are available on the official National Hurricane Center website: National Hurricane Center (NHC), [www.nhc.noaa.gov/verification]

Fujita T., D. J. Stensrud, and D. C. Dowell, 2007: Surface data assimilation using an ensemble Kalman filter approach with initial condition and model physics uncertainties. *Mon. Wea. Rev.,* **135**, 1846-1868.

Gao, J., and M. Xue, 2008: An Efficient Dual-Resolution Approach for Ensemble Data Assimilation and Tests with Simulated Doppler Radar Data. *Mon. Wea. Rev.*, **136**, 945–963.

Houze, R. A., Chen, S.S., Smull, B. F., Lee, W.-C. & Bell, M.M., 2007: Hurricane intensity and eyewall replacement. *Science*, **315**, 1235-1238.

Hendricks E. A., M. T. Montgomery, and C. A. Davis, 2004: The role of "vortical" hot towers in the formation of tropical cyclone Diane (1984). *J. Atmos. Sci.,* **61,** 1209-1232.

Klemp, J. B. and R. B. Wilhelmson, 1978: Simulation of 3-Dimensional convective storm dynamics. *J. Atmos. Sci.,* **35**, 1070-1096.

Knabb, R.D., J.R. Rhome, and D.P. Brown, 2005: Tropical Cyclone Report, Hurricane Katrina, 23-30, August 2005, National Hurricane Center. Online at http://www.nhc.noaa.gov/2005atlan.shtml

Krishnamurti, T.N., and coauthors, 2005: The Hurricane Intensity Issue. *Mon. Wea. Rev*., **133**, 1886-1912.

Kurihara Y., M. A. Bender, and R. J. Ross, 1993: An initialization scheme of hurricane models by vortex specification. *Mon. Wea. Rev.,* **121**, 2030-2045.

Leidner S. M., L. Isaksen, and R. N. Hoffman, 2003: Impact of NSCAT winds on tropical cyclones in the ECMWF 4DVAR assimilation system. *Mon. Wea. Rev.* **131**, 3-26.

Leslie, L. M. and G. J. Holland, 1995: On the bogussing of tropical cyclones in numerical models: A comparison of vortex profiles. *Met. Atmos. Phys.,* **56**, 101-110.

Liu, Y., D. Zhang, and M. K. Yau, 1999: A Multiscale Numerical Study of Hurricane Andrew (1992). Part II: Kinematics and Inner-Core Structure. *Mon. Wea. Rev.,* **127**, 2597-2616.

Meng, Z, and F. Zhang, 2007: Test of an ensemble-Kalman filter for mesoscale and regional- scale data assimilation. Part II: Imperfect-model experiments. *Mon. Wea. Rev*., **135**, 1403-1423.

Meng, Z, and F. Zhang, 2008a: Test of an ensemble-Kalman filter for mesoscale and regional- scale data assimilation. Part III: Comparison with 3Dvar in a real-data case study. *Mon. Wea. Rev*., **136**, 522-540.

Meng, Z, and F. Zhang, 2008b: Test of an ensemble-Kalman filter for mesoscale and regional- scale data assimilation. Part IV: Performance over a warm-season month of June 2003. *Mon. Wea. Rev*., **136**, 3671-

3682.
Montgomery M. T.,M. E. Nicholls, T. A. Cram, and A. B. Saunders, 2006: A vortical hot tower route to tropical cyclogenesis. *J. Atmos. Sci.,* **63**, 355-386.
Pu, Z. X. and S. A. Braun, 2001: Evaluation of bogus vortex techniques with four-dimensional variational data assimilation. *Mon. Wea. Rev.*, **129**, 2023-2039.
Rotunno, R. and K. A. Emanuel, 1987: An air-sea interaction theory for tropical cyclones. Part II: Evolutionary study using a nonhydrostatic axisymmetric numerical model. *J. Atmos. Sci.*, **44**, 542-561.
Shea, D. J. and W. M. Gray, 1973: Hurricanes inner core region. Part I: Symmetric and asymmetric structure. *J. Atmos. Sci.,* **30**, 1544-1564.
Skamarock, W. C., J. B. Klemp, J. Dudhia, D. O. Gill, D. M. Barker, W. Wang, and J. G. Powers, 2005: A description of the advanced research WRF version 2. *NCAR Technical Note*, NCAR/TN-468+STR.
Snyder, C., and F. Zhang, 2003: Tests of an ensemble Kalman filter for convective-scale data assimilation. *Mon. Wea. Rev.*, **131**, 1663-1677.
Talagrand, O., 1997: Assimilation of observations, an introduction. *J. Met. Soc. Japan*, **75**, 191-209.
Tong, M., and M. Xue, 2005: Ensemble Kalman filter assimilation of Doppler Radar data with a compressible nonhydrostatic model: OSS experiments. *Mon. Wea. Rev.,***133**, 1789-1807.
Torn R. D., G. J. Hakim, and C. Snyder, 2006: Boundary conditions for a limited-area ensemble Kalman filter. *Mon. Wea. Rev.*, **134**, 2490-2502.
Torn, R. D. and G. J. Hakim 2009: Ensemble Data Assimilation Applied to RAINEX Observations of Hurricane Katrina (2005). *Mon. Wea. Rev.*, **137**, 2817-2829.
Willoughby, H. E. and coauthors, 1984: Hurricane structure and evolution as simulated by an axisymmetric, nonhydrostatic, numerical-model. *J. Atmos. Sci.,* **41**, 1169-1186.
Wang, B., R. L. Elsberry, Y. Wang, and L. Wu, 1998: Dynamics in tropical cyclone motion: A review. *Chinese J. Atmos. Sci.,* **22**, 535-547.
Wu, C-C, and K. A. Emanuel, 1993: Interaction of a baroclinic vortex with background shear: Application to hurricane movement. *J. Atmos. Sci*., **50**, 62-76.
Wu, C-C, and Y. Kurihara, 1996: A numerical study of the feedback mechanism of hurricane-environment interaction on hurricane movement from the potential vorticity perspective. *J. Atmos. Sci.*, **53**, 2264-2282.
Xiao, Q. N., X. L. Zou, B. Wang, 2000: Initialization and simulation of a landfalling hurricane using a variational bogus data assimilation scheme. *Mon. Wea. Rev.*, **128**, 2252-2269.
Xiao, Q., Y.H. Kuo, J. Sun, W.C. Lee, D.M. Barker, and E. Lim, 2007: An Approach of Radar Reflectivity Data Assimilation and Its Assessment with the Inland QPF of Typhoon Rusa (2002) at Landfall. *J. Appl. Meteor. Climat.*, **46**, 14-22.
Zhang, F., C. Snyder, and J. Sun, 2004: Tests of an ensemble Kalman filter for convective-scale data assimilation: Impact of initial estimate and observations. *Mon. Wea. Rev*., **132**, 1238-1253.
Zhang, F., 2005: Dynamics and structure of mesoscale error covariance of a winter cyclone estimated through short-range ensemble forecasts. *Mon. Wea. Rev*., **133**, 2876-2893.
Zhang, F., Z. Meng and A. Aksoy, 2006: Test of an ensemble-Kalman filter for mesoscale and regional-scale data assimilation. Part I: Perfect-model experiments. *Mon. Wea. Rev*., **134**, 722-736.
Zhang, F. Q. and coauthors, 2009: Cloud-Resolving Hurricane Initialization and Prediction through Assimilation of Doppler Radar Observations with an Ensemble Kalman Filter. *Mon. Wea. Rev.,* **137**, 2105-2125.
Zhang, F. and J. A. Sippel, 2008: Effects of moist convection on hurricane predictability. *J. Atmos. Sci.*, **66**, 1944-1961.
Zou, X., and Q. Xiao, 2000: Studies on the initialization and simulation of a mature hurricane using a variational bogus data assimilation scheme. *J. Atmos. Sci.*, **57**, 836-860.